JOURNAL OF GEOPHYSICAL RESEARCH, VOL. 113, D11212, doi:10.1029/2007JD009017, 2008

Retrieval of X_{CO_2} from simulated Orbiting Carbon Observatory measurements using the fast linearized R-2OS radiative transfer model

Vijay Natraj,[1] Hartmut Boesch,[2,3] Robert J. D. Spurr,[4] and Yuk L. Yung[1]

Received 29 May 2007; revised 23 August 2007; accepted 11 December 2007; published 14 June 2008.

[1] In a recent paper, we introduced a novel technique to compute the polarization in a vertically inhomogeneous, scattering-absorbing medium using a two orders of scattering (2OS) radiative transfer (RT) model. The 2OS computation is an order of magnitude faster than a full multiple scattering scalar calculation and can be implemented as an auxiliary code to compute polarization in operational retrieval algorithms. In this paper, we employ the 2OS model for polarization in conjunction with a scalar RT model (Radiant) to simulate backscatter measurements in near infrared (NIR) spectral regions by space-based instruments such as the Orbiting Carbon Observatory (OCO). Computations are performed for six different sites and two seasons, representing a variety of viewing geometries, surface and aerosol types. The aerosol extinction (at 13000 cm^{-1}) was varied from 0 to 0.3. The radiance errors using the Radiant/2OS (R-2OS) RT model are an order of magnitude (or more) smaller than errors arising from the use of the scalar model alone. In addition, we perform a linear error analysis study to show that the errors in the retrieved column-averaged dry air mole fraction of CO_2 (X_{CO_2}) using the R-2OS model are much lower than the "measurement" noise and smoothing errors appearing in the inverse model. On the other hand, we show that use of the scalar model alone induces X_{CO_2} errors that could dominate the retrieval error budget.

Citation: Natraj, V., H. Boesch, R. J. D. Spurr, and Y. L. Yung (2008), Retrieval of X_{CO_2} from simulated Orbiting Carbon Observatory measurements using the fast linearized R-2OS radiative transfer model, *J. Geophys. Res.*, *113*, D11212, doi:10.1029/2007JD009017.

1. Introduction

[2] Satellite measurements have played a major role in weather and climate research for the past few decades, and will continue to do so in the future. For most remote sensing applications, interpretation of such measurements requires accurate modeling of the interaction of light with the atmosphere and surface. In particular, polarization effects due to the surface, atmosphere and instrument need to be considered. *Aben et al.* [1999] suggested the use of high spectral resolution polarization measurements in the O_2 *A* band for remote sensing of aerosols in the Earth's atmosphere. *Stam et al.* [2000] showed that for polarization-sensitive instruments, the best way to minimize errors in quantities derived from the observed signal is by measuring the state of polarization of the observed light simultaneously with the radiances themselves. *Hasekamp et al.* [2002] demonstrated the need to model polarization effects in ozone profile retrieval algorithms based on moderate-resolution backscattered sunlight measurements in the ultraviolet (UV). *Jiang et al.* [2004] proposed a method to retrieve tropospheric ozone from measurements of linear polarization of scattered sunlight from the ground or from a satellite.

[3] Typically, trace gas retrieval algorithms neglect polarization in the forward model radiative transfer (RT) simulations, mainly because of insufficient computer resources and lack of speed. This can result in significant loss of accuracy in retrieved trace gas column densities, particularly in the UV, visible and near infrared (NIR) spectral regions, because of appreciable light scattering by air molecules, aerosols and clouds. It has been shown that neglecting polarization in a Rayleigh scattering atmosphere can produce errors as large as 10% in the computed intensities [*Mishchenko et al.*, 1994; *Lacis et al.*, 1998].

[4] The inclusion of polarization in forward modeling has been handled by methods such as the use of lookup tables [*Wang*, 2006], or the combination of limited polarization measurement data with interpolation schemes [*Schutgens and Stammes*, 2003]. Such methods have been implemented with reasonable success for certain applications. However,

[1]Division of Geological and Planetary Sciences, California Institute of Technology, Pasadena, California, USA.
[2]Jet Propulsion Laboratory, California Institute of Technology, Pasadena, California, USA.
[3]Now at Department of Physics and Astronomy, University of Leicester, Leicester, UK.
[4]RT Solutions Inc., Cambridge, Massachusetts, USA.

0148-0227/08/2007JD009017$09.00

there are situations where the required retrieval precision is very high, so that such simplifications will fail to provide sufficient accuracy. For instance, it has been shown that retrieving the sources and sinks of CO_2 on regional scales requires the column density to be known to 2.5 ppmv (0.7%) precision to match the performance of the existing ground-based network [*Rayner and O'Brien*, 2001] and to 1 ppmv (0.3%) to reduce flux uncertainties by 50% [*Miller et al.*, 2007]. Recent improvements in sensor technology are making very high precision measurements feasible for space-based remote sensing. Clearly, there is a need for polarized RT models that are not only accurate enough to achieve high retrieval precision, but also fast enough to meet operational requirements regarding the rate of data turnover.

[5] In a recent paper [*Natraj and Spurr*, 2007], we presented the theoretical formulation for the simultaneous computation of the top of the atmosphere (TOA) reflected radiance and the corresponding weighting function fields using a two orders of scattering (2OS) RT model. In this paper, we apply the 2OS polarization model in conjunction with the full multiple scattering scalar RT model Radiant [*Benedetti et al.*, 2002; *Christi and Stephens*, 2004; *Gabriel et al.*, 2006; *Spurr and Christi*, 2007] for the simulation of polarized backscatter measurements $\mathbf{I} = (I, Q, U, V)$ in the spectral regions to be measured by the Orbiting Carbon Observatory (OCO) mission [*Crisp et al.*, 2004]. I, Q, U and V are the Stokes parameters [*Stokes*, 1852], which describe the polarization state of electromagnetic radiation. I refers to the total intensity, Q and U are measures of linear polarization, and V describes the state of circular polarization. $\mathbf{I}$ is the Stokes vector. The purpose of the 2OS model is to supply a correction to the total scalar intensity delivered by Radiant, and to compute the other elements (Q, U, V) in the backscatter Stokes vector. The 2OS model provides a fast and accurate way of accounting for polarization in the OCO forward model. The Radiant/2OS (R-2OS) combination thus obviates the need for prohibitively slow full vector multiple scatter simulations.

[6] The R-2OS scheme is a simplification of the forward model. For the OCO retrieval error budget, it is important to quantify the errors in the retrieved column-averaged dry air mole fraction of CO_2 (X_{CO_2}) and ancillary state vector elements such as surface pressure induced by this forward model assumption. The magnitude of the forward model errors are established as the differences between total backscatter radiances from the R-2OS forward model and those calculated by means of the full vector RT model VLIDORT [*Spurr*, 2006]. In order to ensure consistency, we note that the Radiant model as used in the OCO retrieval algorithm has been fully validated against the scalar LIDORT code [*Spurr et al.*, 2001; *Spurr*, 2002] and also VLIDORT operating in scalar mode (polarization turned off); this validation is discussed by *Spurr and Christi* [2007].

[7] The paper is organized as follows. In section 2, we give a brief description of the 2OS model. In section 3, we describe the test scenarios and introduce the solar and instrument models. The spectral radiance errors are analyzed in section 4. In section 5, we study the usefulness of the R-2OS model for CO_2 retrievals by calculating X_{CO_2} errors using a linear sensitivity analysis procedure. We conclude with an evaluation of the implication of these results for the OCO mission in section 6.

2. The 2OS Model

[8] Multiple scattering is known to be depolarizing [*Hansen*, 1971; *Hansen and Travis*, 1974]. However, ignoring polarization in the RT modeling leads to two types of error. First, polarization components (Q, U, V) of the Stokes vector are neglected and will therefore be unknown sources of error in any retrievals using polarized backscatter measurements. The second type of error is in the intensity itself: the scalar value is different from the intensity component of the Stokes vector calculated with polarization included in the RT calculation. The significance of the second kind of error is that even if the instrument were completely insensitive to polarization, errors would still accrue if polarization were neglected in the RT model.

[9] A single scattering RT model provides the simplest approximation to the treatment of polarization. However, for unpolarized incident light, polarization effects on the intensity are absent in this approximation. Hence, the second type of error mentioned above would remain unresolved with this approximation. RT models with three (and higher) orders of scattering give highly accurate results, but involve nearly as much computation as that required for a full multiple scattering treatment (see, e.g., *Kawabata and Ueno* [1988] for the scalar three-orders case). The 2OS treatment represents a good compromise between accuracy and speed when dealing with polarized RT.

[10] In our 2OS model, the computational technique is a vector treatment extension (to include polarization) of previous work done for a scalar model [*Kawabata and Ueno*, 1988]. Full details of the mathematical setup are given elsewhere [*Natraj and Spurr*, 2007]. The following relation summarizes the approach:

$$\begin{pmatrix} I \\ Q \\ U \\ V \end{pmatrix} \cong \begin{pmatrix} I_{sca} \\ 0 \\ 0 \\ 0 \end{pmatrix} + \begin{pmatrix} I_{cor} \\ Q_{2OS} \\ U_{2OS} \\ V_{2OS} \end{pmatrix}, \tag{1}$$

where I, Q, U and V are the Stokes parameters, and subscripts *sca* and *2OS* refer to a full multiple scattering scalar RT calculation and to a vector computation using the 2OS model, respectively. I_{cor} is the scalar-vector intensity correction computed using the 2OS model. Note that the 2OS calculation only computes correction terms due to polarization; a full multiple scattering scalar computation is still required to compute the intensity.

[11] The advantage of this technique is that it is fully based on the underlying physics and is in no way empirical. If the situation were such that two (or lower) orders of scattering are sufficient to account for polarization, this method would be exact. There are some situations, such as an optically thick pure Rayleigh medium or an atmosphere with large aerosol or ice cloud scattering, where the approach will fail. However, for most NIR retrievals, this is likely to be a very accurate approximation. Validation of the 2OS model has been done against scalar results for an

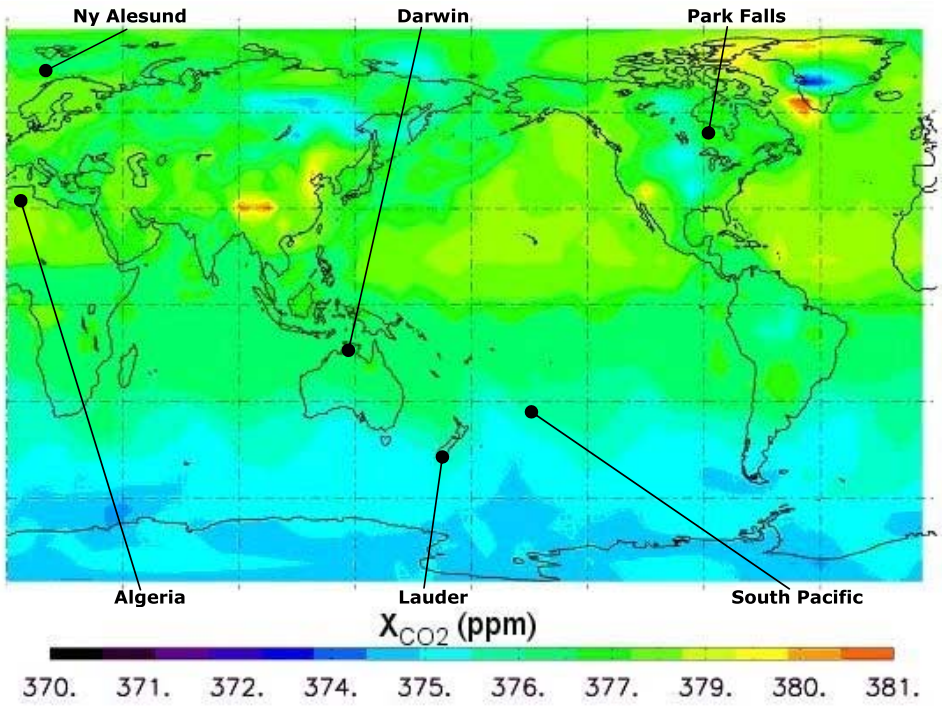

Figure 1. Geographical location map of test sites. The color bar denotes X_{CO_2} for 1 July (1200 UT) calculated using the MATCH/CASA model [*Olsen and Randerson*, 2004]. The coordinates of the locations are as follows: Ny Alesund (79°N, 12°E), Park Falls (46°N, 90°W), Algeria (30°N, 8°E), Darwin (12°S, 130°E), South Pacific (30°S, 210°E) and Lauder (45°S, 170°E).

inhomogeneous atmosphere [*Kawabata and Ueno*, 1988] and vector results for a homogeneous atmosphere [*Hovenier*, 1971]. In the earlier work [*Natraj and Spurr*, 2007], we performed backscatter simulations of reflected sunlight in the O_2 *A* band for a variety of geometries, and compared our results with those from the VLIDORT model. In these simulations, the effects of gas absorption optical depth, solar zenith angle, viewing geometry, surface reflectance and wind speed (in the case of ocean glint) on the intensity, polarization and corresponding weighting functions were investigated. Finally, we note that the 2OS model is completely linearized; that is, the weighting functions or Jacobians (analytic derivatives of the radiance field with respect to atmospheric and surface properties) are simultaneously computed along with the radiances themselves.

3. Simulations

[12] In this work, we use the spectral regions to be measured by the OCO instrument to test the 2OS model. This includes the 0.76 μm O_2 *A* band, and two vibration-rotation bands of CO_2 at 1.61 μm and 2.06 μm [*Kuang et al.*, 2002]. Six different locations and two seasons were considered for the simulations (see Figure 1 for geographical location map). These six sites are all part of the ground-based validation network for the OCO instrument [*Crisp et al.*, 2006; *Washenfelder et al.*, 2006; *Bösch et al.*, 2006]. For each location/season combination, 12 tropospheric aerosol loadings were specified (extinction optical depths 0, 0.002, 0.005, 0.008, 0.01, 0.02, 0.03, 0.04, 0.05, 0.1, 0.2, 0.3 at 13000 cm^{-1}). Details of the geometry, surface and tropospheric aerosol types for the various scenarios are summarized in Table 1.

[13] The atmosphere comprises 11 optically homogeneous layers, each of which includes gas molecules and aerosols. The 12 pressure levels are regarded as fixed, and the altitude grid is computed recursively using the hydrostatic approximation. Spectroscopic data are taken from the HITRAN 2004 molecular spectroscopic database [*Rothman et al.*, 2005]. The tropospheric aerosol types have been chosen according to the climatology developed by *Kahn et al.* [2001]. The stratospheric aerosol is assumed to be a 75% solution of H_2SO_4 with a modified gamma function size distribution [*World Climate Research Programme*, 1986]. The complex refractive index of the sulfuric acid solution is taken from the tables prepared by *Palmer and Williams* [1975]. For spherical aerosol particles, the optical properties are computed using a polydisperse Mie scattering code [*de Rooij and van der Stap*, 1984]; in addition to extinction and scattering coefficients and distribution parameters, this code generates coefficients for the expansion of the scattering matrix in generalized spherical functions (a requirement of all the RT models used in this study). For nonspherical aerosols such as mineral dust, optical properties are computed using a *T* matrix code [*Mishchenko and Travis*, 1998]. The atmosphere is bounded below by a Lambertian reflecting surface. The surface reflectances are taken from the ASTER spectral library (http://speclib.jpl.nasa.gov). Note that all RT models in this paper use a pseudo-spherical approximation, in which all scattering is regarded as taking place in a plane-parallel medium, but the solar beam attenuation is treated for a curved atmosphere. The pseudo-

Table 1. Scenario Description[a]

	Solar Zenith Angle, deg	Surface Type	Aerosol Type [*Kahn et al.*, 2001]
Algeria 1 Jan	57.48	desert (0.42, 0.5, 0.53)	dusty continental (4b)
Algeria 1 Jul	21.03	desert (0.42, 0.5, 0.53)	dusty continental (4b)
Darwin 1 Jan	23.24	deciduous (0.525, 0.305, 0.13)	dusty maritime (1a)
Darwin 1 Jul	41.44	deciduous (0.525, 0.305, 0.13)	black carbon continental (5b)
Lauder 1 Jan	34.22	grass (0.47, 0.3, 0.11)	dusty maritime (1a)
Lauder 1 Jul	74.20	frost (0.975, 0.305, 0.145)	dusty maritime (1b)
Ny Alesund 1 Apr	80.77	snow (0.925, 0.04, 0.0085)	dusty maritime (1b)
Ny Alesund 1 Jul	62.43	grass (0.47, 0.3, 0.11)	dusty maritime (1b)
Park Falls 1 Jan	72.98	snow (0.925, 0.04, 0.0085)	black carbon continental (5b)
Park Falls 1 Jul	31.11	conifer (0.495, 0.235, 0.095)	dusty continental (4b)
South Pacific 1 Jan	24.62	ocean (0.03, 0.03, 0.03)	dusty maritime (1a)
South Pacific 1 Jul	58.84	ocean (0.03, 0.03, 0.03)	dusty maritime (1b)

[a]The surface reflectances in the O_2 *A* band, 1.61 μm CO_2 band and 2.06 μm CO_2 band are given in parentheses after the surface type. For the aerosol types, the values in parentheses are the mixing groups assigned by *Kahn et al.* [2001].

spherical treatment is based on the average-secant approximation [see, e.g., *Spurr*, 2002].

[14] The OCO instrument is a polarizing spectrometer measuring backscattered sunlight in the O_2 *A* band, and the CO_2 bands at 1.61 μm and 2.06 μm [*Haring et al.*, 2004, 2005; *Crisp et al.*, 2006]. OCO is scheduled for launch in December 2008, and will join NASA's "A-train" along a sun-synchronous polar orbit with 1326 local equator crossing time (ascending node), about 5 min ahead of the Aqua platform [*Crisp et al.*, 2006]. OCO is designed to operate in three modes: nadir, glint (utilizing specular reflection over the ocean) and target (to stare over a fixed spot, such as a validation site), and has a nominal spatial footprint dimension of 1.3 km × 2.3 km in the nadir mode. The OCO polarization axis is always perpendicular to the principal plane, so that the backscatter measurement is, in terms of Stokes parameters, equal to *I*-*Q*.

[15] In the OCO retrieval algorithm, the complete forward model describes all physical processes pertaining to the attenuation and scattering of sunlight through the atmosphere (including reflection from the surface) to the instrument. Thus, the forward model consists of the RT model, a solar model and an instrument model. The R-2OS RT model computes a monochromatic top-of-atmosphere

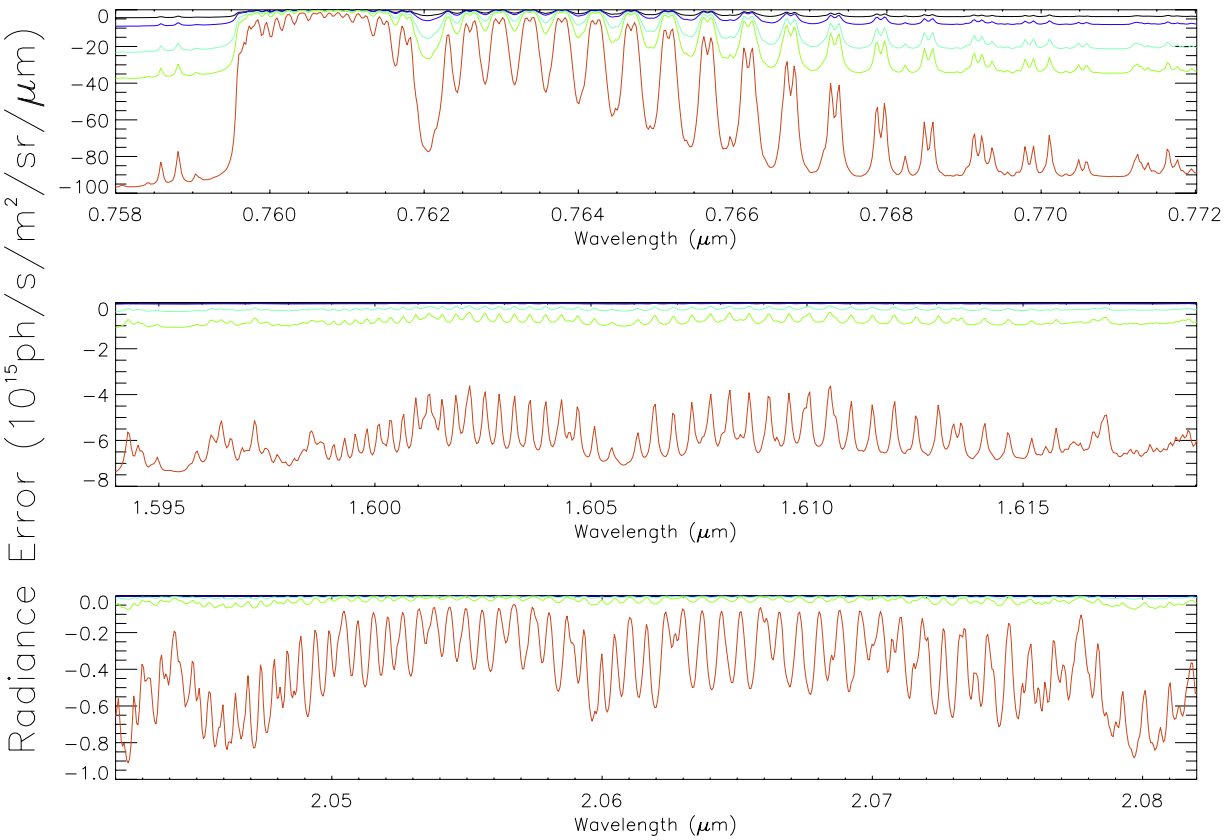

Figure 2. Radiance errors using the R-2OS model for South Pacific in January. The black, blue, cyan, green and red lines refer to aerosol extinction optical depths (at 13000 cm^{-1}) of 0, 0.01, 0.05, 0.1 and 0.3, respectively. (top) The O_2 *A* band, (middle) the 1.61 μm CO_2 band and (bottom) the 2.06 μm CO_2 band.

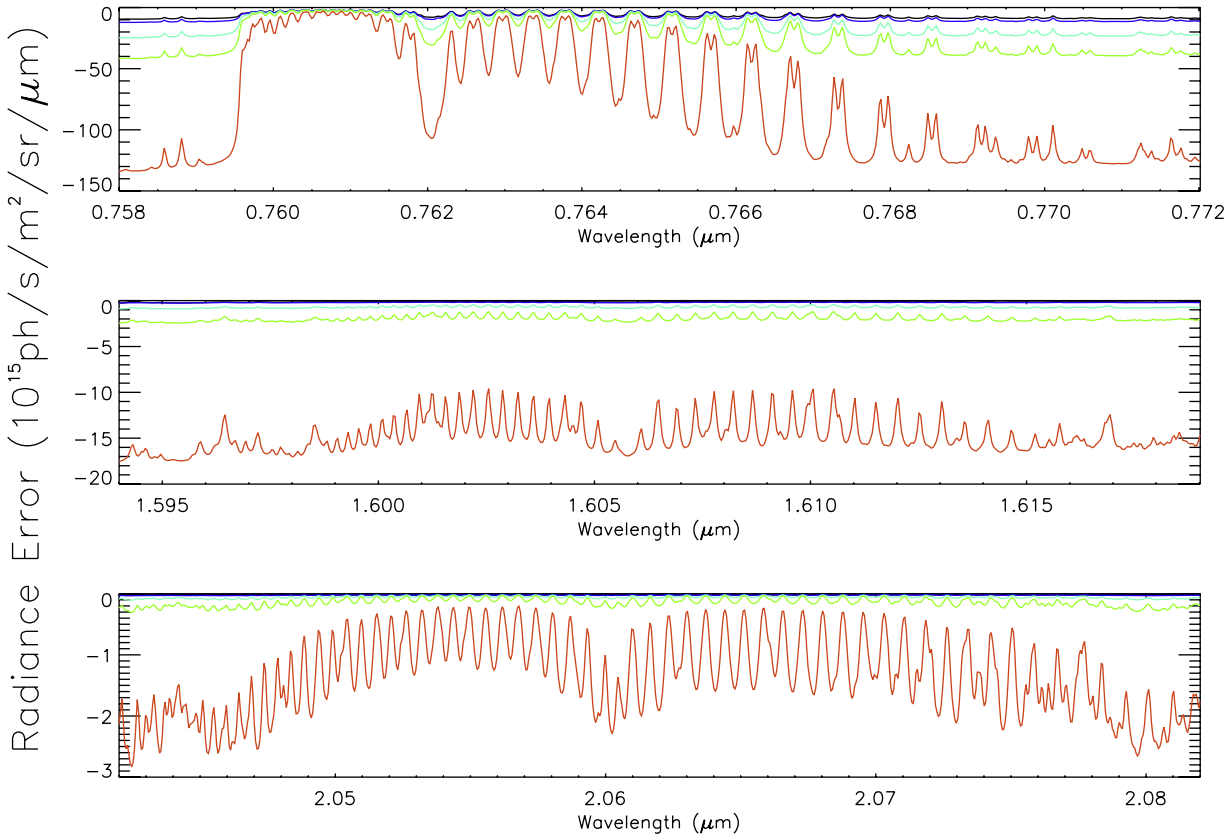

Figure 3. Same as Figure 2 but for Algeria in January.

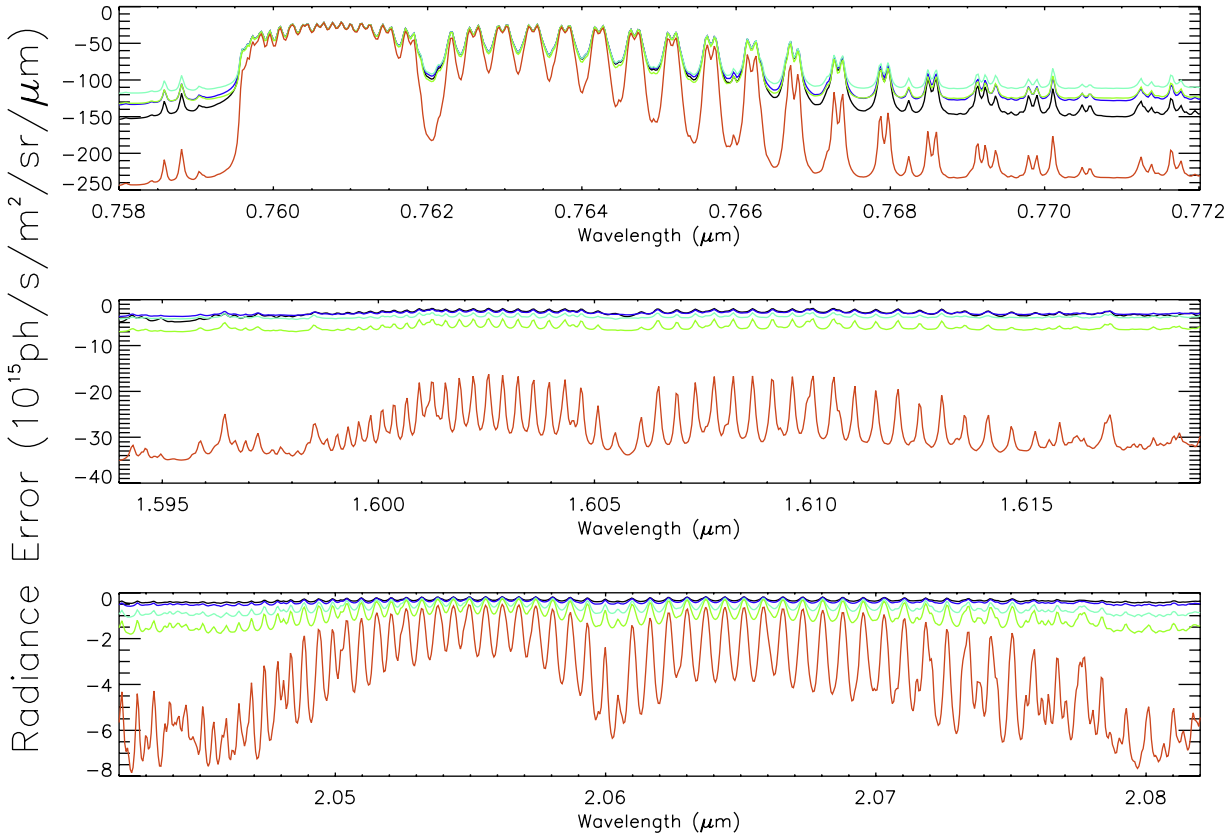

Figure 4. Same as Figure 2 but for Ny Alesund in April.

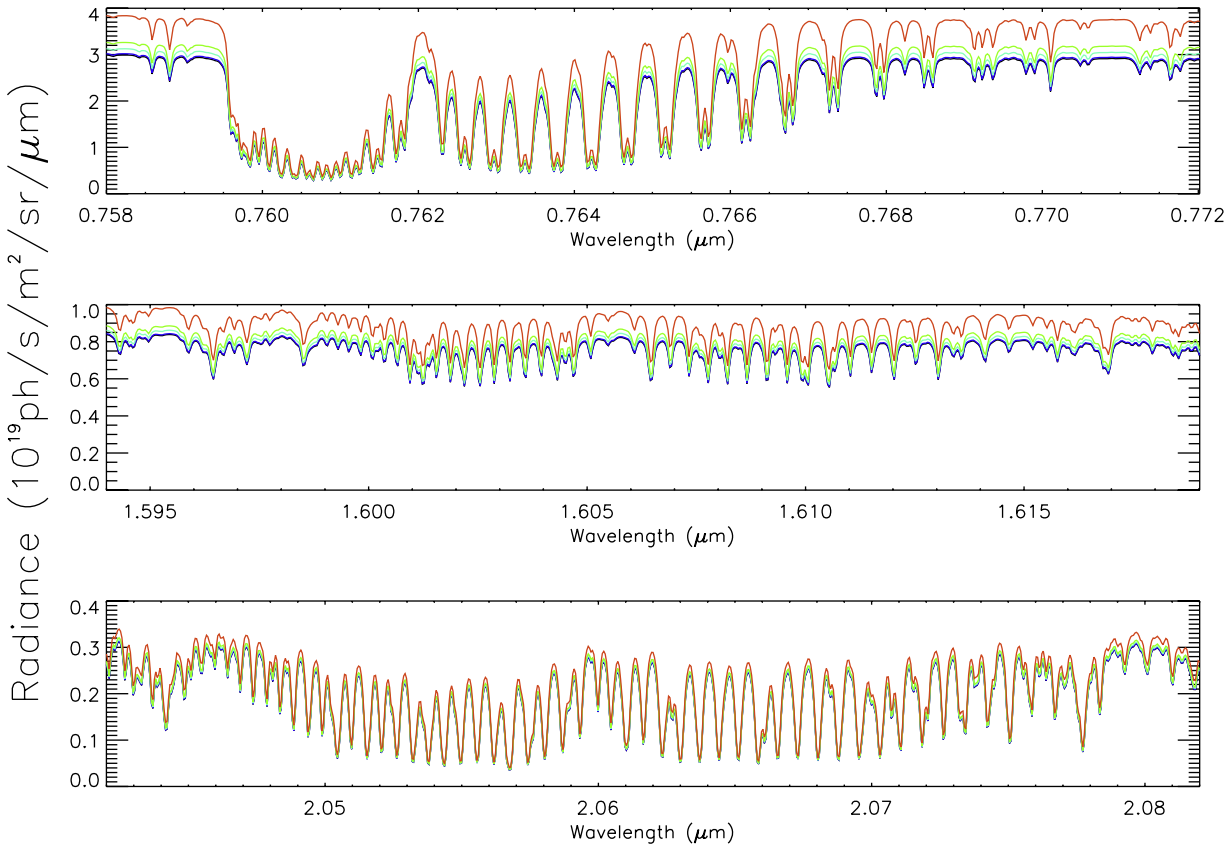

Figure 5. "Exact" radiance spectra for South Pacific in January. The black, blue, cyan, green and red lines refer to aerosol extinction optical depths (at 13000 cm^{-1}) of 0, 0.01, 0.05, 0.1 and 0.3, respectively. (top) The O_2 *A* band, (middle) the 1.61 μm CO_2 band and (bottom) the 2.06 μm CO_2 band.

(TOA) reflectance spectrum at a wave number resolution of 0.01 cm^{-1}; this is sufficient to resolve the individual O_2, CO_2 and H_2O lines in the OCO spectral regions with 5–8 points per Lorentz full-width for typical surface conditions and at least 2 points throughout the troposphere. The OCO solar model is based on an empirical list of solar line parameters which allows computation of a solar spectrum with arbitrary spectral resolution and point spacing [*Bösch et al.*, 2006]. The instrument model simulates the instrument's spectral resolution and spectral sampling by convolving the highly resolved monochromatic radiance spectrum with the instrument line shape function (ILS), and subsequently with a boxcar function to take into account the spectral range covered by a detector pixel. The ILS is assumed to be Lorentzian with Half Width at Half Maximum (HWHM) 2.25 $\times$ 10^{-5} μm, 4.016 $\times$ 10^{-5} μm and 5.155 $\times$ 10^{-5} μm for the 0.76 μm O_2 *A* band, 1.61 μm CO_2 band and 2.06 μm CO_2 band, respectively.

4. Forward Model Uncertainties

[16] For the three OCO spectral bands, Figures 2–4 show the forward model radiance errors caused by the R-2OS model. Results are shown for July scenarios in South Pacific (Figure 2), Algeria (Figure 3) and Ny Alesund (Figure 4). These are scenarios with low solar zenith angle and low surface reflectance, low solar zenith angle and moderate surface reflectance, and high solar zenith angle, respectively. The errors in the O_2 *A* band, the 1.61 μm CO_2 band and 2.06 μm CO_2 band are plotted in the top, middle and bottom panels, respectively. The black, blue, cyan, green and red lines refer to aerosol extinction optical depths (at 13000 cm^{-1}) of 0, 0.01, 0.05, 0.1 and 0.3, respectively. In calculating these errors, the "exact" radiance is taken to be that computed with VLIDORT. The "exact" radiance spectra for the July scenario in South Pacific are plotted in Figure 5.

[17] The plots reveal a number of interesting features. It is clear that the errors in the O_2 *A* band are orders of magnitude larger than those in the CO_2 bands; this is not surprising, since scattering is a much bigger issue in the O_2 *A* band. Further, the spectral error behavior is different for the three cases. For low solar zenith angle and moderate to high surface reflectance (Figure 3), scattering first increases as gas absorption increases with line strength; this is on account of the corresponding reduction in the amount of light directly reflected from the surface. With a further enhancement of gas absorption, a point is reached where the effect of the surface becomes negligibly small, and any subsequent increase in gas absorption leads to a reduction in the orders of scattering. Consequently, there is a maximum error in the intensity when the orders of scattering are maximized. For Stokes parameter *Q*, this effect would not show up since there is no contribution from (Lambertian) reflection at the surface. Further, for small angles, the intensity effect dominates over the *Q* effect and the radiance errors show a maximum at intermediate gas absorption. If

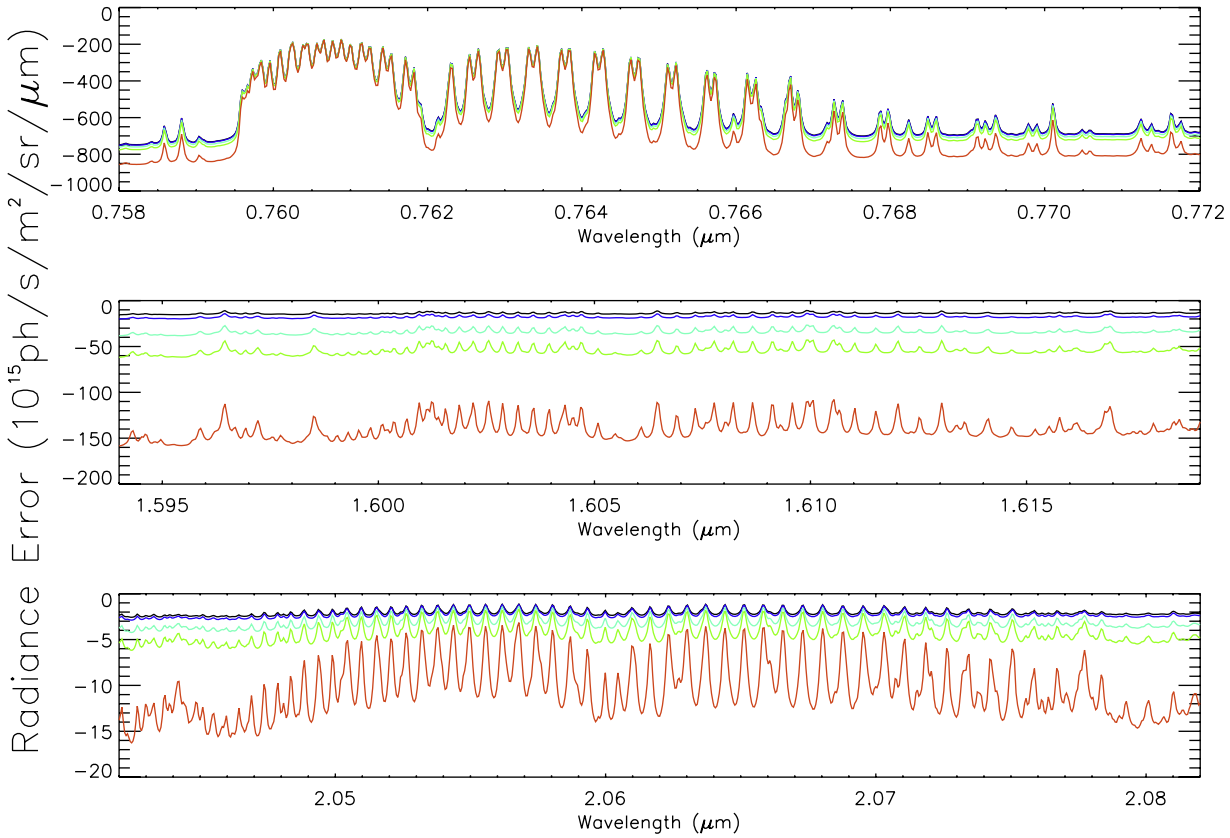

Figure 6. Same as Figure 2 but for radiance errors using the scalar model.

the surface reflectance is reduced to a low level (Figure 2), the effect of direct reflected light becomes very small, and the I and Q errors behave similarly, with the result that the errors are maximized when gas absorption is at a minimum. The same effect occurs if the solar zenith angle is increased (Figure 4). Increasing aerosol extinction reduces the surface contribution; hence, the spectral behavior for high aerosol amounts is the same as that for low surface reflectance or high solar zenith angle.

[18] On the other hand, the errors (at constant gas absorption) increase with augmenting aerosol extinction, except in the high solar zenith angle case (Figure 4), where they decrease at first and reach minimum values for certain low aerosol amounts. This special case can be explained as follows. Small aerosol amounts have the effect of reducing the contribution of Rayleigh scattering relative to aerosol scattering. The former is conservative, while the latter is not. The net effect is that scattering is reduced. However, at a certain point, the contribution from Rayleigh scattering becomes insignificant, and further increase in aerosol extinction simply increases the overall scattering and the level of error.

[19] For the January scenarios (not plotted here), the spectral error behavior generally follows the pattern discussed above. The only exception is Darwin (tropical Australia), where the error initially decreases as aerosol is added, even though the solar zenith angle is small. This is because Darwin has been assigned a continental aerosol type with significant amounts of carbonaceous and black carbon components [*Kahn et al.*, 2001], both of which are strongly absorbing. This has the effect of reducing scattering up to the point where Rayleigh scattering is no longer significant.

[20] The radiance errors caused by the scalar model have been investigated before [*Natraj et al.*, 2007]; it was shown that they could be as high as 300% (relative to the full vector calculation). The corresponding errors introduced by the R-2OS model are typically in the range of 0.1% (see, e.g., Figures 2 and 5). For the scenario in Figure 2, spectral radiance errors using only the scalar Radiant model (without 2OS) are plotted in Figure 6. It is immediately apparent that the errors from the scalar model are an order of magnitude (or more) larger than those induced by the R-2OS model. Further, the Radiant-only errors primarily arise from neglecting the polarization caused by Rayleigh and aerosol scattering; hence, they are sensitive to the particular type of aerosol present in the scenario. For example, the errors in the O_2 A band decrease with an increase in tropospheric aerosol for the Park Falls and Darwin July scenarios (not plotted here). These cases are characterized by aerosols that polarize in the p plane at the scattering angles of interest, whereas Rayleigh scattering is s polarized. In some cases (such as Algeria in July), the error actually changes sign for large aerosol extinction. To a large extent, the R-2OS model removes this sensitivity to aerosol type.

5. Linear Sensitivity Analysis

[21] From a carbon source-sink modeling standpoint, it is important to understand the effect of the R-2OS approximation on the accuracy of the retrieved CO_2 column. The

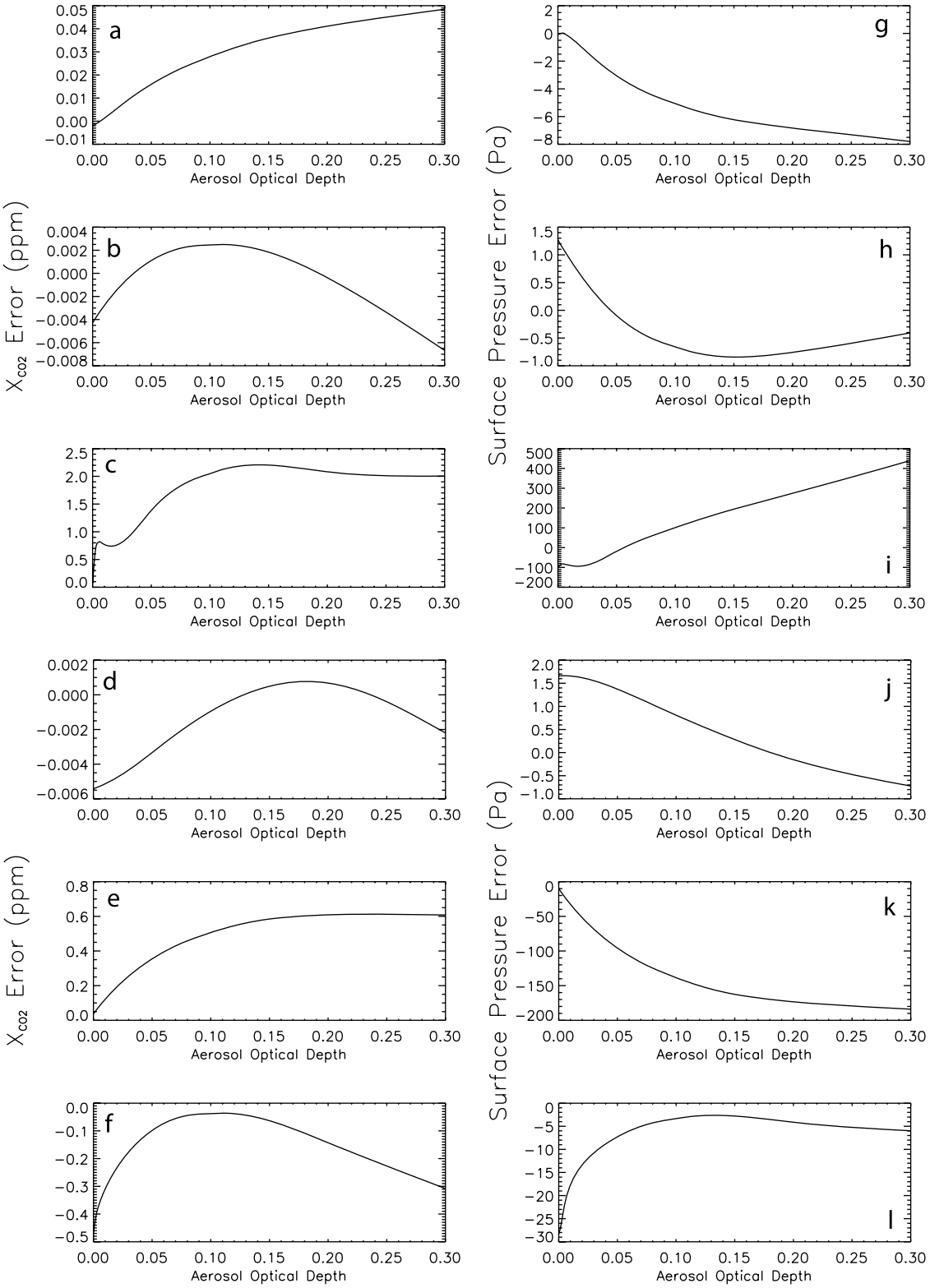

Figure 7. (a–f) X_{CO_2} and (g–l) surface pressure errors using the R-2OS model. Shown are Algeria (Figures 7a and 7g) and Darwin (Figures 7b and 7h) in January and Ny Alesund in April (Figures 7c and 7i). Also shown are Lauder (Figures 7d and 7j), South Pacific (Figures 7e and 7k) and Park Falls (Figures 7f and 7l) in January.

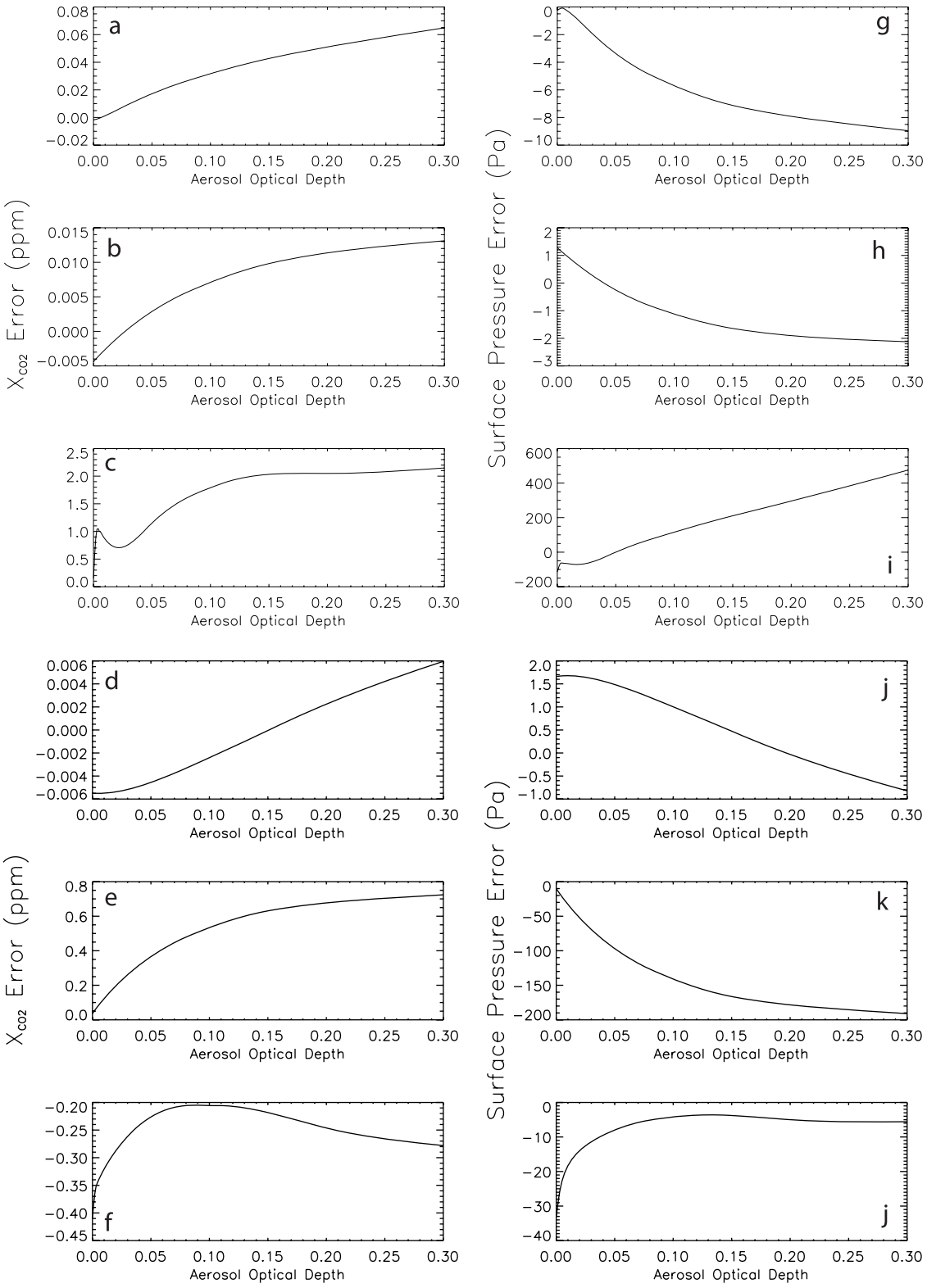

Figure 8. Same as Figure 7 but assuming that the only radiance error contribution is from the O_2 *A* band.

linear error analysis technique [*Rodgers*, 2000] can be used to quantify biases caused by uncertainties in nonretrieved forward model parameters (such as absorption cross sections), or by inadequacies in the forward model itself (such as the R-2OS approximation). Here we perform this linear error analysis using the inverse model in the OCO Level 2 retrieval algorithm [*Bösch et al.*, 2006; *Connor et al.*, 2008].

[22] The retrieval algorithm iteratively adjusts a set of atmospheric/surface/instrument parameters by alternate calls to a forward model and an inverse method. The

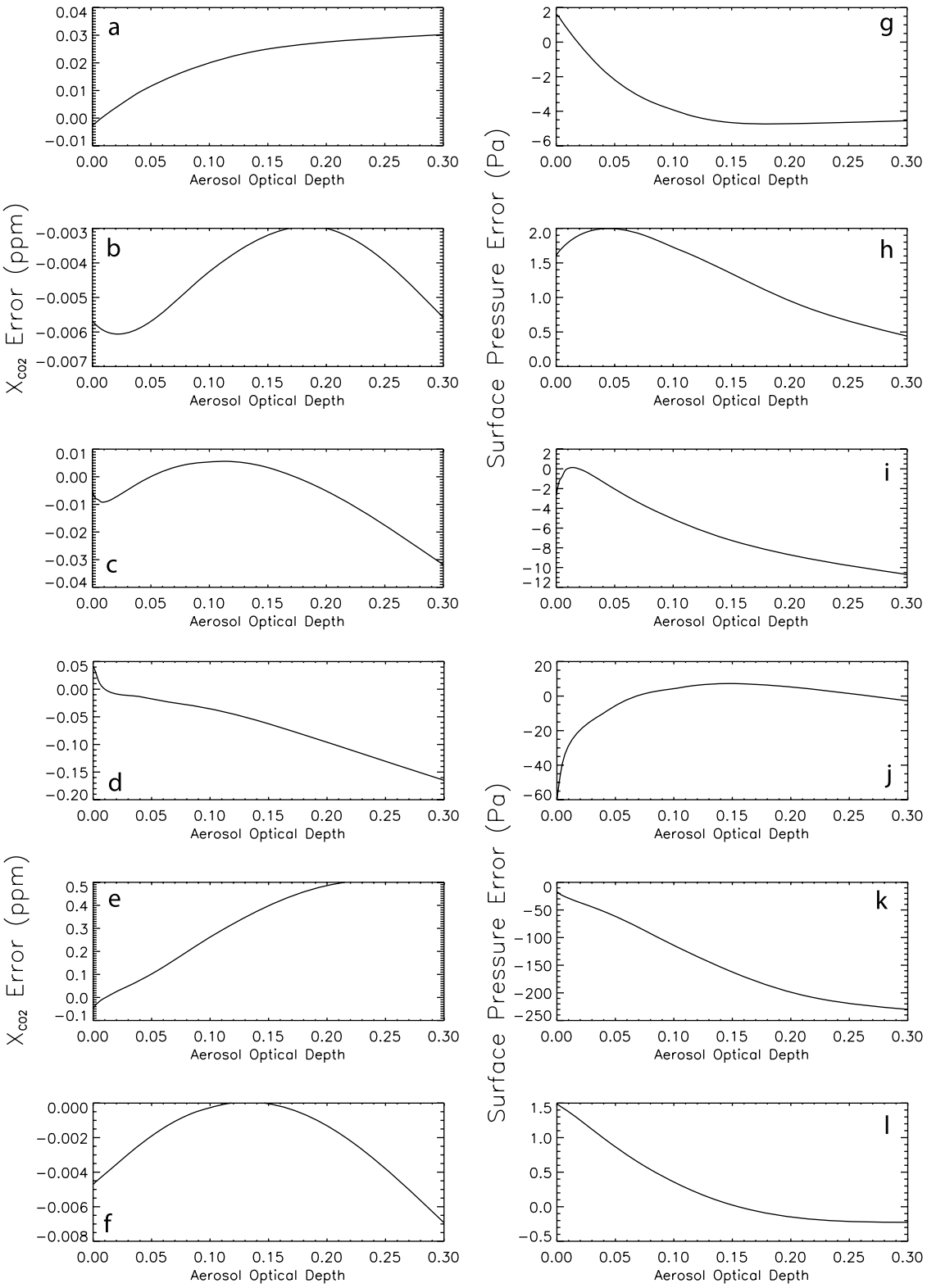

Figure 9. Same as Figure 7 but for July.

measurement **y** can be simulated by a forward model f(**x**):

$$\mathbf{y} = f(\mathbf{x}, \mathbf{b}) + \varepsilon, \tag{2}$$

where **x** and **b** represent retrieved and nonretrieved forward model parameters, respectively, and ε is the measurement noise.

[23] In the OCO retrieval algorithm, the inverse method is based on optimal estimation [*Rodgers*, 2000] and uses a priori information to constrain the retrieval problem. The a priori data provide information about the climatological mean and expected variability of the relevant quantities. Weighting functions describing the change of the "mea-

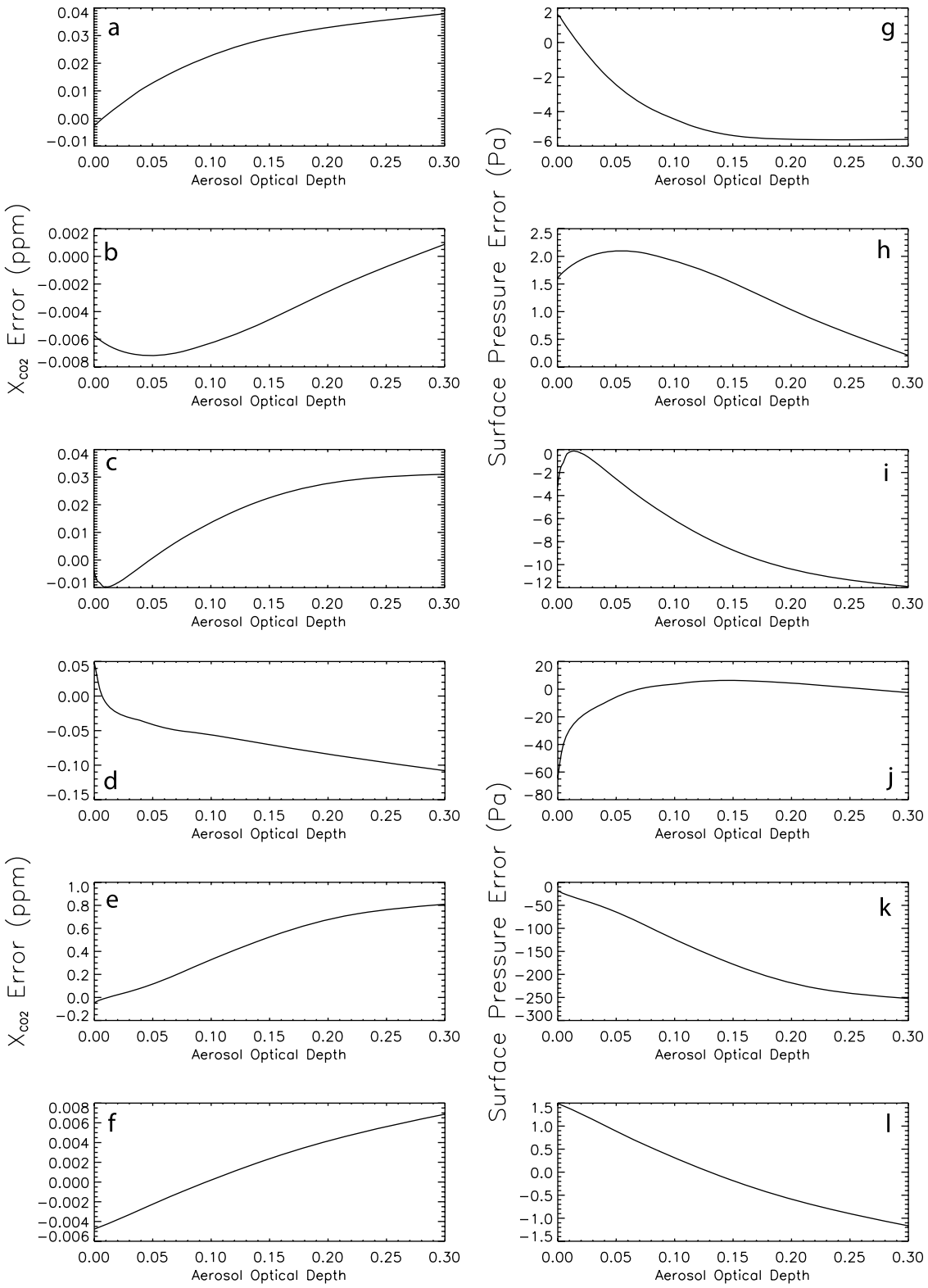

Figure 10. Same as Figure 8 but for July.

sured'' spectrum with respect to a change in the retrieved parameters are calculated analytically by repeated calls to the linearized R-2OS model. The OCO algorithm simultaneously fits the spectra of the 3 absorption bands, and retrieves a set of 61 parameters for a 12-level atmosphere. These retrieved elements consist of 4 vertical profiles (CO_2 volume mixing ratio (vmr), H_2O vmr, temperature and aerosol extinction optical depth), as well as a number of other elements including surface pressure, surface reflectance and its spectral dependence, spectral shift and

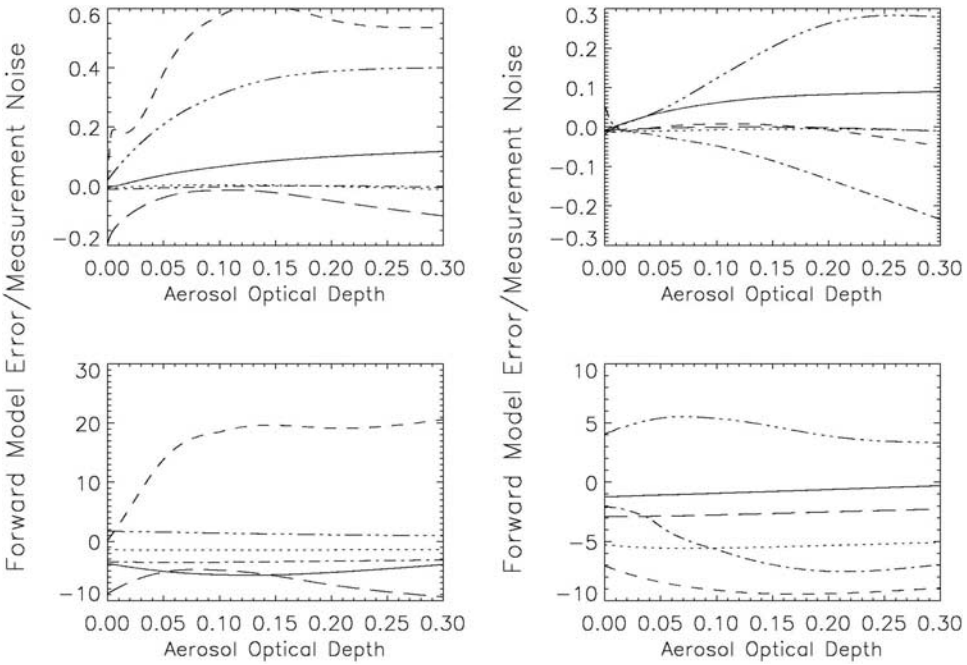

Figure 11. Ratio of forward model error to "measurement" noise using the (a and b) R-2OS model and (c and d) scalar model. The solid, dotted, dashed, dash-dotted, dash-dot-dot-dotted and long dashed lines refer to Algeria and Darwin in January (Figures 11a and 11c) and July (Figures 11b and 11d); Ny Alesund in April (Figures 11a and 11c) and July (Figures 11b and 11d); and Lauder, South Pacific, and Park Falls in January (Figures 11a and 11c) and July (Figures 11b and 11d), respectively.

squeeze/stretch. Optimal estimation involves minimizing a regularized cost function χ^2:

$$\chi^2 = [\mathbf{y} - f(\mathbf{x})]^T \mathbf{S}_\varepsilon^{-1} [\mathbf{y} - f(\mathbf{x})] + (\mathbf{x} - \mathbf{x}_a)^T \mathbf{S}_a^{-1} (\mathbf{x} - \mathbf{x}_a), \quad (3)$$

where $\mathbf{x}_a$ is the a priori state vector, $\mathbf{S}_a$ is the a priori covariance matrix and $\mathbf{S}_e$ is the measurement error covariance matrix. The measurement errors are assumed to have no correlation between different detector pixels; that is, $\mathbf{S}_e$ is a diagonal matrix. The superscript T indicates the transpose of the vector.

[24] The column-weighted CO_2 vmr X_{CO_2} is given by:

$$X_{CO_2} = \mathbf{h}^T \mathbf{x}, \quad (4)$$

where $\mathbf{h}$ is the pressure weighting operator [*Connor et al.*, 2008], whose elements are zero for all non-CO_2 elements. Clearly, X_{CO_2} depends on the surface pressure and the CO_2 vmr profile.

[25] In the error analysis, we apply the OCO inverse model once to a set of simulated spectra calculated assuming that the state vector is the truth; that is, we assume that the iterative retrieval scheme has already converged. The retrieval and smoothing errors and the gain matrix are calculated by the retrieval algorithm. The smoothing error describes the error in the retrieved parameters due to the limited sensitivity of the retrieval to fine structures of atmospheric profiles. The analysis of smoothing errors requires knowledge about the real atmospheric variability; we use an a priori CO_2 covariance that represents a total, global variability of 12 ppmv to avoid overconstraining the retrieval [*Connor et al.*, 2008]. Consequently, the calculated smoothing errors will represent a global upper limit. For all other retrieval parameters, ad hoc a priori constraints are used, with no cross correlation between different parameters.

[26] Forward model errors are typically systematic and result in a bias $\Delta\mathbf{x}$ in the retrieved parameters. This bias can be expressed as:

$$\Delta\mathbf{x} = \mathbf{G}\Delta\mathbf{F}, \quad (5)$$

where $\mathbf{G}$ is the gain matrix, that represents the mapping of the measurement variations into the retrieved state vector variations, and $\Delta\mathbf{F}$ is the vector of radiance errors made using the R-2OS model. Since OCO measures perpendicular to the principal plane, $\Delta\mathbf{F}$ has the following component at wave number ν_j corresponding to the jth detector pixel:

$$[\Delta\mathbf{F}]_j = \big(I(\nu_j) - Q(\nu_j)\big) - \big(I_{vec}(\nu_j) - Q_{vec}(\nu_j)\big), \quad (6)$$

where the subscript *vec* refers to a full vector multiple scattering calculation.

[27] The X_{CO_2} errors using the R-2OS model for the January and July scenarios are presented in Figures 7 and 8, respectively. Figures 7 and 8 also show the corresponding errors in surface pressure. With very few exceptions, the X_{CO_2} errors are very small and much below the OCO precision requirement of 1 ppmv. This is in contrast to the observation that ignoring polarization generates errors that could dominate the error budget for many scenarios [*Natraj et al.*, 2007].

[28] To understand the error trend, we also plot the errors in X_{CO_2} and surface pressure assuming that there is no radiance error in the CO_2 absorption bands (Figures 9 and 10). X_{CO_2} errors have contributions from errors in surface pressure and CO_2 vmr. The former is primarily due to radiance errors in the O_2 *A* band, while the latter comes from incorrectly evaluating the radiances in the 1.61 μm CO_2 band. There are also cross correlations between the two. It is evident from Figures 7–10 that the X_{CO_2} errors mirror the surface pressure errors for low aerosol amounts. This is to be expected since the maximum radiance errors are in the O_2 *A* band, as previously noted. As we increase the aerosol extinction, the errors in the CO_2 bands start to become more significant. The turnaround at large aerosol extinction optical depths is because of the competing effects of surface pressure and CO_2 vmr errors. In addition, as expected, there is an inverse correlation between X_{CO_2} and surface pressure errors. The only exceptions are the winter scenarios in Ny Alesund and Park Falls. These cases have surface type snow, which is extremely bright in the O_2 *A* band and extremely dark in the CO_2 bands. The very low albedo in the 1.61 μm CO_2 band causes significant polarization and gives rise to positive pressure partials; that is, the TOA radiance increases as we increase surface pressure.

[29] The ratio of forward model (FM) error to ''measurement'' noise is plotted in Figure 11, with the top and bottom rows referring to the R-2OS and scalar models, respectively. The R-2OS forward model error is typically less than 20% of the noise error and only in a few cases exceed 50%. In contrast, errors using the scalar model exceed unity in almost all cases and can be up to 20 times larger. The behavior of the smoothing errors is very similar and is not plotted here.

6. Conclusions

[30] For high-resolution accurate forward modeling in remote sensing applications, we have developed a joint RT model (R-2OS) which computes intensities using a scalar multiple scattering model along with corrections for polarization effects by means of a two orders of scattering RT code. The R-2OS model was employed to simulate backscatter measurements of spectral bands by the OCO instrument. A variety of scenarios was considered, representing different viewing geometries, surface and aerosol types, and aerosol extinctions. It was found that the errors in the radiance were an order of magnitude or more less than the errors when polarization was neglected. Further, the error characteristics were largely independent of the aerosol type.

[31] Sensitivity studies were performed to evaluate the errors in the retrieved CO_2 column resulting from using the R-2OS model. It was seen that the X_{CO_2} errors using the R-2OS model were much lower than the smoothing error and ''measurement'' noise. This is in contrast to the observation that the retrieval error budget could be potentially dominated by polarization if the scalar model was used. The retrieval error was dominated by incorrect estimation of the surface pressure (due to radiance errors in the O_2 *A* band), with other effects becoming important for large aerosol amounts. It is worth noting that the 2OS computation adds about 10% to the RT calculation time.

[32] **Acknowledgments.** The research described in this paper was performed for the Orbiting Carbon Observatory Project at the Jet Propulsion Laboratory, California Institute of Technology, under contracts with NASA. This work was supported in part by NASA grant NAG1-1806. The authors would like to thank Hari Nair for assistance with the forward model and error analysis simulations; Ralph Kahn for discussions on aerosols; Michael Mishchenko, Joop Hovenier and Johan de Haan for providing *T* matrix and Mie codes; Dave Crisp for assistance with detector optics; Run-Lie Shia and Dan Feldman for helpful comments on the manuscript; and two anonymous reviewers for suggestions to revise the manuscript.

References

Aben, I., F. Helderman, D. M. Stam, and P. Stammes (1999), Spectral fine-structure in the polarisation of skylight, *Geophys. Res. Lett.*, *26*(5), 591–594, doi:10.1029/1999GL900025.

Benedetti, A., P. Gabriel, and G. L. Stephens (2002), Properties of reflected sunlight derived from a Green's function method, *J. Quant. Spectrosc. Radiat. Transfer*, *72*(3), 201–225, doi:10.1016/S0022-4073(01)00055-3.

Bösch, H., et al. (2006), Space-based near-infrared CO_2 measurements: Testing the Orbiting Carbon Observatory retrieval algorithm and validation concept using SCIAMACHY observations over Park Falls, Wisconsin, *J. Geophys. Res.*, *111*, D23302, doi:10.1029/2006JD007080.

Christi, M. J., and G. L. Stephens (2004), Retrieving profiles of atmospheric CO_2 in clear sky and in the presence of thin cloud using spectroscopy from the near and thermal infrared: A preliminary case study, *J. Geophys. Res.*, *109*, D04316, doi:10.1029/2003JD004058.

Connor, B. J., H. Boesch, G. Toon, B. Sen, C. Miller, and D. Crisp (2008), Orbiting Carbon Observatory: Inverse method and prospective error analysis, *J. Geophys. Res.*, *113*, D05305, doi:10.1029/2006JD008336.

Crisp, D., et al. (2004), The Orbiting Carbon Observatory (OCO) mission, *Adv. Space Res.*, *34*(4), 700–709, doi:10.1016/j.asr.2003.08.062.

Crisp, D., C. E. Miller, and P. L. DeCola (2006), The NASA Orbiting Carbon Observatory: Measuring the column-averaged atmospheric CO_2 mole fraction abundance from space, in *Proc. SPIE, Sensors, Systems, and Next-Generation Satellites X*, *6361*, 63610H, R. Meynart, S. P. Neeck, and H. Shimoda (Eds.), doi:10.1117/12.689570.

de Rooij, W. A., and C. C. A. H. van der Stap (1984), Expansion of Mie scattering matrices in generalized spherical functions, *Astron. Astrophys.*, *131*(2), 237–248.

Gabriel, P., M. Christi, and G. L. Stephens (2006), Calculation of Jacobians for inverse radiative transfer: An efficient hybrid method, *J. Quant. Spectrosc. Radiat. Transfer*, *97*(2), 209–227, doi:10.1016/j.jqsrt.2005.05.060.

Hansen, J. E. (1971), Multiple scattering of polarized light in planetary atmospheres. Part II. Sunlight reflected by terrestrial water clouds, *J. Atmos. Sci.*, *28*(8), 1400–1426, doi:10.1175/1520-0469(1971)028<1400:MSOPLI>2.0.CO;2.

Hansen, J. E., and L. D. Travis (1974), Light scattering in planetary atmospheres, *Space Sci. Rev.*, *16*(4), 527–610, doi:10.1007/BF00168069.

Haring, R., R. Pollock, B. M. Sutin, and D. Crisp (2004), The Orbiting Carbon Observatory instrument optical design, in *Proc. SPIE - Current Developments in Lens Design and Optical Engineering V*, *5523*, P. Z. Mouroulis, W. J. Smith, and R. B. Johnson (Eds.), 51–62, doi:10.1117/12.562693.

Haring, R., R. Pollock, B. M. Sutin, and D. Crisp (2005), Current development status of the Orbiting Carbon Observatory instrument optical design, *Proc. SPIE Int. Soc. Opt. Eng.*, *5883*, 61–70, doi:10.1117/12.617706.

Hasekamp, O. P., J. Landgraf, and R. F. van Oss (2002), The need of polarization modeling for ozone profile retrieval from backscattered sunlight, *J. Geophys. Res.*, *107*(D23), 4692, doi:10.1029/2002JD002387.

Hovenier, J. W. (1971), Multiple scattering of polarized light in planetary atmospheres, *Astron. Astrophys.*, *13*, 7–29.

Jiang, Y., Y. L. Yung, S. P. Sander, and L. D. Travis (2004), Modeling of atmospheric radiative transfer with polarization and its application to the remote sensing of tropospheric ozone, *J. Quant. Spectrosc. Radiat. Transfer*, *84*(2), 169–179, doi:10.1016/S0022-4073(03)00140-7.

Kahn, R., P. Banerjee, and D. McDonald (2001), Sensitivity of multiangle imaging to natural mixtures of aerosols over ocean, *J. Geophys. Res.*, *106*(D16), 18,219–18,238, doi:10.1029/2000JD900497.

Kawabata, K., and S. Ueno (1988), The first three orders of scattering in vertically inhomogeneous scattering-absorbing media, *Astrophys. Space Sci.*, *150*(2), 327–344, doi:10.1007/BF00641728.

Kuang, Z., J. S. Margolis, G. C. Toon, D. Crisp, and Y. L. Yung (2002), Spaceborne measurements of atmospheric CO_2 by high-resolution NIR spectrometry of reflected sunlight: An introductory study, *Geophys. Res. Lett.*, *29*(15), 1716, doi:10.1029/2001GL014298.

Lacis, A. A., J. Chowdhary, M. I. Mishchenko, and B. Cairns (1998), Modeling errors in diffuse-sky radiation: Vector vs. scalar treatment, *Geophys. Res. Lett.*, *25*(2), 135–138, doi:10.1029/97GL03613.

Miller, C. E., et al. (2007), Precision requirements for space-based X_{CO_2} data, *J. Geophys. Res.*, *112*, D10314, doi:10.1029/2006JD007659.

Mishchenko, M. I., and L. D. Travis (1998), Capabilities and limitations of a current Fortran implementation of the *T*-matrix method for randomly oriented, rotationally symmetric scatterers, *J. Quant. Spectrosc. Radiat. Transfer*, *60*(3), 309–324, doi:10.1016/S0022-4073(98)00008-9.

Mishchenko, M. I., A. A. Lacis, and L. D. Travis (1994), Errors induced by the neglect of polarization in radiance calculations for Rayleigh-scattering atmospheres, *J. Quant. Spectrosc. Radiat. Transfer*, *51*(3), 491–510, doi:10.1016/0022-4073(94)90149-X.

Natraj, V., and R. J. D. Spurr (2007), A fast linearized pseudo-spherical two orders of scattering model to account for polarization in vertically inhomogeneous scattering-absorbing media, *J. Quant. Spectrosc. Radiat. Transfer*, *107*(2), 263–293, doi:10.1016/j.jqsrt.2007.02.011.

Natraj, V., R. J. D. Spurr, H. Bösch, Y. Jiang, and Y. L. Yung (2007), Evaluation of errors from neglecting polarization in the analysis of O2 A band measurements from space, *J. Quant. Spectrosc. Radiat. Transfer*, *103*(2), 245–259, doi:10.1016/j.jqsrt.2006.02.073.

Olsen, S. C., and J. T. Randerson (2004), Differences between surface and column atmospheric CO_2 and implications for carbon cycle research, *J. Geophys. Res.*, *109*, D02301, doi:10.1029/2003JD003968.

Palmer, K. F., and D. Williams (1975), Optical constants of sulfuric acid; application to the clouds of Venus?, *Appl. Opt.*, *14*(1), 208–219.

Rayner, P. J., and D. M. O'Brien (2001), The utility of remotely sensed CO_2 concentration data in surface source inversions, *Geophys. Res. Lett.*, *28*(1), 175–178, doi:10.1029/2000GL011912.

Rodgers, C. D. (2000), *Inverse Methods for Atmospheric Sounding: Theory and Practice*, World Sci., Singapore.

Rothman, L. S., et al. (2005), The HITRAN 2004 molecular spectroscopic database, *J. Quant. Spectrosc. Radiat. Transfer*, *96*(2), 139–204, doi:10.1016/j.jqsrt.2004.10.008.

Schutgens, N. A. J., and P. Stammes (2003), A novel approach to the polarization correction of spaceborne spectrometers, *J. Geophys. Res.*, *108*(D7), 4229, doi:10.1029/2002JD002736.

Spurr, R. J. D. (2002), Simultaneous derivation of intensities and weighting functions in a general pseudo-spherical discrete ordinate radiative transfer treatment, *J. Quant. Spectrosc. Radiat. Transfer*, *75*(2), 129–175, doi:10.1016/S0022-4073(01)00245-X.

Spurr, R. J. D. (2006), VLIDORT: A linearized pseudo-spherical vector discrete ordinate radiative transfer code for forward model and retrieval studies in multilayer multiple scattering media, *J. Quant. Spectrosc. Radiat. Transfer*, *102*(2), 316–342, doi:10.1016/j.jqsrt.2006.05.005.

Spurr, R. J. D., and M. J. Christi (2007), Linearization of the interaction principle: Analytic Jacobians in the "Radiant" model, *J. Quant. Spectrosc. Radiat. Transfer*, *103*(3), 431–446, doi:10.1016/j.jqsrt.2006.05.001.

Spurr, R. J. D., T. P. Kurosu, and K. V. Chance (2001), A linearized discrete ordinate radiative transfer model for atmospheric remote-sensing retrieval, *J. Quant. Spectrosc. Radiat. Transfer*, *68*(6), 689–735, doi:10.1016/S0022-4073(00)00055-8.

Stam, D. M., J. F. De Haan, J. W. Hovenier, and I. Aben (2000), Detecting radiances in the O_2 *A* band using polarization-sensitive satellite instruments with application to the Global Ozone Monitoring Experiment, *J. Geophys. Res.*, *105*(D17), 22,379–22,392, doi:10.1029/2000JD900313.

Stokes, G. G. (1852), On the composition and resolution of streams of polarized light from different sources, *Trans. Cambridge Philos. Soc.*, *9*, 399–416.

Wang, M. (2006), Aerosol polarization effects on atmospheric correction and aerosol retrievals in ocean color remote sensing, *Appl. Opt.*, *45*(35), 8951–8963, doi:10.1364/AO.45.008951.

Washenfelder, R. A., et al. (2006), Carbon dioxide column abundances at the Wisconsin tall tower site, *J. Geophys. Res.*, *111*, D22305, doi:10.1029/2006JD007154.

World Climate Research Programme (1986), A preliminary cloudless standard atmosphere for radiation computation, *Rep. WCP-112*, World Meteorol. Organ., Geneva, Switzerland.

H. Boesch, Department of Physics and Astronomy, University of Leicester, Leicester LE1 7RH, UK.

V. Natraj and Y. L. Yung, Division of Geological and Planetary Sciences, California Institute of Technology, MC 150-21, Pasadena, CA 91125, USA. (vijay@gps.caltech.edu)

R. J. D. Spurr, RT Solutions Inc., 9 Channing Street, Cambridge, MA 02138, USA.